

PERMANENT-MAGNET MICROSTRUCTURES FOR ATOM OPTICS*

A.I. SIDOROV^(a), R.J. MCLEAN^(a), F. SCHARNBERG^(a), D.S. GOUGH^(a)
T.J. DAVIS^(b), B.J. SEXTON^(b), G.I. OPAT^{(c)†} AND P. HANNAFORD^(a)

^(a)Centre for Atom Optics and Ultrafast Spectroscopy
Swinburne University of Technology, Hawthorn, Victoria 3122, Australia

^(b)CSIRO Manufacturing Science and Technology
Clayton, Victoria 3169, Australia

^(c)School of Physics, The University of Melbourne, Victoria 3010, Australia

(Received June 3, 2002)

We describe the use of permanent magnetic microstructures based on grooved, perpendicularly magnetised thin films fabricated by electron-beam lithography as optical elements for atom optics. Strong reflection signals and predominantly specular reflection have been realised for beams of cold caesium or rubidium atoms normally incident on grooved perpendicularly magnetised microstructures with periodicities of 1–4 μm . We discuss the use of perpendicularly magnetised microstructures to construct miniature integrated atom optical elements, including magnetic waveguides, microtraps and beamsplitters, for manipulating atomic de Broglie waves on the surface of a substrate.

PACS numbers: 03.75.Be, 32.80.Pj, 32.80.Lg

1. Introduction

High-quality atomic optical elements including mirrors, beamsplitters and waveguides are needed for reflecting, coherently splitting, and transporting beams of slowly moving atoms in a variety of atom optics applications including atom interferometry. An approach which we are investigating makes use of the interaction of the atom's magnetic dipole moment with the exponentially decaying magnetic field above a periodic array of magnets of alternating polarity [1], in which the decay length is determined by the periodicity of the array. When slowly moving atoms in low field-seeking magnetic

* Presented at the Photons, Atoms and All That, PAAT 2002 Conference, Cracow Poland, May 31–June 1, 2002.

† Deceased 7 March, 2002.

states approach the surface of the magnetic structure, they are repelled by the increasing magnetic field strength, and the structure may behave as an atomic mirror [1–3]. Proposed schemes for fabricating magnetic mirrors include recording periodic magnetic fields on ferromagnetic substrates as in sound recording [1] and constructing planar arrays of parallel wires alternately carrying electric currents in opposite directions [1]. Such magnetic optical elements are static, robust and miniature, and may be suitable for portable sensing devices such as gravimeters and gravity gradiometers.

A periodic magnetic structure may be converted into a diffraction grating, or diffractive beamsplitter, for slowly moving atoms by applying a small bias magnetic field perpendicular to the surface of the structure to form a spatial grating [1, 4], or by vibrating the magnetic structure or applying an oscillating orthogonal magnetic field to form a temporal grating or “acousto-optic modulator” for atoms [5]. A periodic magnetic structure may be turned into a magnetic tube for guiding atoms by forming a cylindrical surface with the direction of magnetisation along the axis of the cylinder [6]. A cylindrical surface consisting of a double-helix solenoid with two identical interwoven solenoids carrying equal currents in opposite directions [7,8] may also be used as a guiding tube for slowly moving atoms.

In practice, the periodicity of the magnetic structure needs to be small, preferably of the order of a micron, to produce a “hard” magnetic mirror and short decay length (and hence large magnetic field gradient) with minimal “end-effects”, and to allow the construction of a spatial diffraction grating (beamsplitter) with reasonably large diffraction angles or a temporal diffraction grating with reasonable diffraction intensities [5]. The challenge is to be able to fabricate magnetic structures with periodicity as small as a micron that will specularly reflect slowly moving atoms. To date, approaches used to produce magnetic microstructures include recording of structures on conventional magnetic media [2, 9, 10], and on magneto-optical films using a tightly focussed laser beam [11, 12], and constructing periodic arrays of current-carrying wires [13, 14]. Magnetic structures recorded on conventional magnetic media appear to be limited to periodicities of order $10\ \mu\text{m}$ and by inhomogeneities in the magnetic media [10], structures recorded on magneto-optical film have to date been limited by break-up of the premagnetised regions during the recording process [15], while periodic structures based on current-carrying conductors have been limited by current density considerations to periodicities of about $50\ \mu\text{m}$ [13, 14].

In this paper we report the use of permanent magnetic microstructures based on *grooved*, magnetic films as optical elements for atom optics. Such grooved magnetic structures may be fabricated with micron-scale periodicity and excellent definition and surface topology using electron-beam lithography and replication techniques. Our earlier attempts to fabricate such

magnetic microstructures from ferromagnetic nickel, cobalt or AlNiCo magnetised in-plane proved to be unsuccessful owing to the difficulty in magnetising the thin films between the grooves of the microstructure [11, 16]. We have since found that by using materials that can be magnetised in the perpendicular direction, such as $\text{Co}_{0.8}\text{Cr}_{0.2}$, it is possible to fabricate high-quality magnetic microstructures with periodicity down to a micron. Preliminary results of this work have been reported elsewhere [15].

In the second part of this paper we discuss the use of perpendicularly magnetised microstructures to construct miniature integrated atom optical elements, including magnetic waveguides, microtraps and beamsplitters, for manipulating atomic de Broglie waves on the surface of a substrate [17]. Structures based on permanent magnetic films have potential advantages over current-carrying devices [18]: they can allow larger magnetic field gradients (potentially $\sim 10^8$ G/cm), and hence tighter confinement of the atoms, without excessive heating or potential breakdown of the current-carrying circuits, and they allow higher stability and less noise owing to the absence of electric currents.

2. Periodic grooved magnetic microstructures

2.1. Physical principles

We consider an atom with magnetic dipole moment $\boldsymbol{\mu}$ moving in an inhomogeneous magnetic field $\mathbf{B}(x, y, z)$. If the rate of change of $\mathbf{B}(x, y, z)$ as seen by the moving atom is slow compared with the atom's Larmor frequency, then the orientation of $\boldsymbol{\mu}$ adiabatically follows the direction of the magnetic field. The position-dependent interaction potential $U_{\text{int}}(x, y, z) = -\boldsymbol{\mu} \cdot \mathbf{B}(x, y, z)$ then exerts a gradient force $\mathbf{F}_{\text{grad}} = \nabla(\boldsymbol{\mu} \cdot \mathbf{B}) = -mg_{\text{F}}\mu_{\text{B}}\nabla B(x, y, z)$ on the atom, where m is the magnetic quantum number, g_{F} is the Landé factor, and μ_{B} the Bohr magneton. Thus atoms in low field-seeking magnetic states ($mg_{\text{F}} > 0$) experience a repulsive force when moving in an increasing magnetic field. Use of the Stern–Gerlach gradient magnetic force has been demonstrated for a beam of laser-cooled atoms moving in the inhomogeneous magnetic field created by a single current-carrying wire [19].

For an infinite periodic array of long magnets of alternating perpendicular magnetisation $M(x) = +M_0$ and $-M_0$ (Fig. 1(a)), the magnetic field strength at distance y above the array is given by [20, 21]

$$|B(x, y)| = B_0 e^{-ky} \left[\left(1 - e^{-kb}\right) + \frac{1}{3} \left(1 - e^{-3kb}\right) e^{-2ky} \cos 2kx + \dots \right], \quad (1)$$

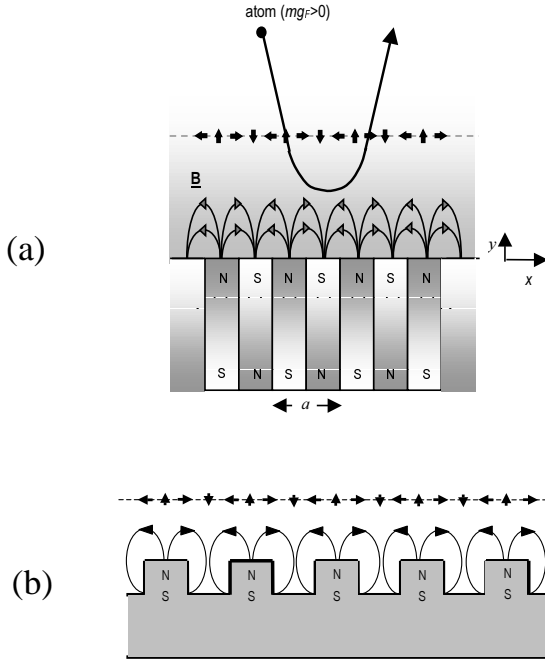


Fig. 1. Schematic diagram of (a) a magnetic mirror consisting of a periodic array of perpendicularly magnetised elements of alternating polarity, (b) a grooved perpendicularly magnetised microstructure.

where $k^{-1} = a/2\pi$ is the decay length, a is the periodicity, $B_0 = 2\mu_0 M_0/\pi$ is a characteristic surface magnetic field, and the factors $(1 - e^{-kb})$, *etc.* take account of the finite thickness b of the magnets. For distances $y > a/4\pi$ above the array and thick magnets ($b \gg a/2\pi$), the components of the magnetic field are given by [21]

$$B_x(x, y) \approx -B_0 e^{-ky} \cos kx, \tag{2a}$$

$$B_y(x, y) \approx B_0 e^{-ky} \sin kx \tag{2b}$$

and the magnetic field strength by

$$|B(y)| \approx B_0 e^{-ky}. \tag{2c}$$

Under these conditions, the magnitude of the magnetic field is independent of the coordinate x and falls off exponentially with distance y above the surface with decay length $a/2\pi$, while the direction of the magnetic field

for a given y rotates in the xy -plane with period a . The third- and higher-order spatial harmonics in (1) contribute a corrugation, which for atoms of mass M dropped from height h has a relative amplitude given to good approximation by

$$C \approx \frac{1}{3} \left[\frac{Mgh}{mg_{\text{F}}\mu_{\text{B}}B_0} \right]^2. \quad (3)$$

For a *grooved* periodic magnetic structure with perpendicular magnetisation in the y direction (Fig. 1(b)), model calculations show that the magnetic field distribution is the same as for a periodic array of magnets of alternating polarity, but with the magnetic field strength reduced by a factor of two. Thus, for a grooved magnetic structure the characteristic surface magnetic field B_0 in (1) and (2) is replaced by $B'_0 = \mu_0 M_0 / \pi$. For a grooved magnetic structure with in-plane magnetisation in the x direction, the magnetic field distribution is the same as for perpendicular magnetisation except the expressions (2a) and (2b) for $B_x(x, y)$ and $B_y(x, y)$ are interchanged.

2.2. Model calculations of grooved magnetic microstructures

Model calculations, in which each magnet in the periodic structure is represented by a pair of sheets of current flowing in opposite directions, were performed for various configurations of grooved magnetic structure. For the magnetic structure in Fig. 2 with $a = 1 \mu\text{m}$, $b = 0.2 \mu\text{m}$, $d = 0.5 \mu\text{m}$, $M_0 = 5 \text{ kG}$ and dimensions $15 \text{ mm} \times 15 \text{ mm}$, the characteristic surface magnetic field is $B'_0 = 1.1 \text{ kG}$, compared with the value 1.25 kG for the case of an infinite array of thick magnets with large groove depth. The model calculations show that for ^{87}Rb atoms dropped from a height $h = 17 \text{ mm}$ onto such a microstructure, the atoms see a corrugation with period a and relative amplitude at the turning point of $\Delta B/B = 0.0016$, which is due largely to “end-effects” arising from the finite number (15,000) of periods in the magnetic structure. The corrugations due to such end-effects can be compensated by applying a small bias magnetic field (43 mG for the above case)

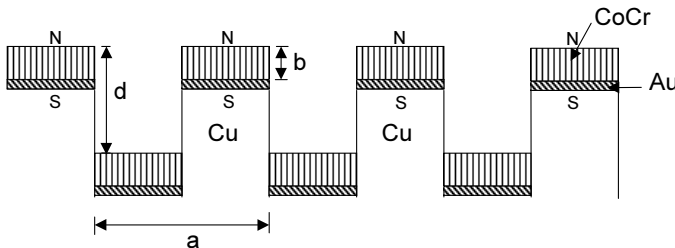


Fig. 2. Geometry of the grooved perpendicularly magnetised CoCr microstructure.

normal to the surface. A bias magnetic field may also be used to compensate for stray magnetic fields, which need to be less than about 10 mG to keep $\Delta\theta_{\text{rms}} < 1$ mrad. The residual corrugation is then $\Delta B/B = 0.0003$ (with period $a/2$), which is due to the third-order spatial harmonic in (2). This residual corrugation leads to an estimated angular spread $\Delta\theta_{\text{rms}} \approx 0.2$ mrad, allowing for integration over the atom's path. The above calculation assumes uniformly magnetised elements and grooves with perfectly straight walls.

2.3. Fabrication of grooved magnetic microstructures

Periodic grooved microstructures with periodicities of $a = 0.7, 1, 2$ and $4 \mu\text{m}$, groove depth $d = 0.6 \mu\text{m}$, and dimensions $15 \text{ mm} \times 15 \text{ mm}$ were written in photoresist by electron-beam lithography, and a nickel master was made from the patterned photoresist using electro-plating techniques. A $0.12 \mu\text{m}$ -thick film of gold was electron-beam evaporated onto a passivated nickel submaster coated with a 50 nm -thick adhesive film of titanium/titanium oxide, and a thick ($\sim 2 \text{ mm}$) supporting layer of copper was electro-plated over the gold, allowing the replication of a non-magnetic grooved Au/Cu substrate. A $0.2 \mu\text{m}$ -thick film of ferromagnetic $\text{Co}_{0.8}\text{Cr}_{0.2}$ was then dc-sputtered onto the grooved Au/Cu replica, which was maintained at 200°C to allow the $\text{Co}_{0.8}\text{Cr}_{0.2}$ film to grow with its easy axis of magnetisation in the perpendicular direction. Finally, the $\text{Co}_{0.8}\text{Cr}_{0.2}$ microstructures were cut to the required size ($10 \text{ mm} \times 9 \text{ mm}$) with a KrF excimer laser beam and magnetised in the direction perpendicular to the surface to form grooved magnetic microstructures similar to Fig. 2.

2.4. Characterisation of the grooved magnetic microstructures

Fig. 3(a) shows Atomic Force Microscope (AFM) and Magnetic Force Microscope (MFM) scans taken at a constant height $y \approx 0.05 \mu\text{m}$ above the tops of the grooves of the magnetised $\text{Co}_{0.8}\text{Cr}_{0.2}$ microstructures. The grooves are represented by the dark regions in the AFM scans and by the light regions in the MFM scans. The MFM scans show that the variation of B_y with x has a phase $n\pi$ (but not $n\pi/2$) relative to the grooved structure, indicating that the grooved structures have been successfully magnetised in the perpendicular direction. Three-dimensional MFM scans (Fig. 4) show that the variation of B_y with x is approximately sinusoidal even at distances very close ($y \approx 0.05 \mu\text{m}$) to the surface. The approximate sinusoidal shape is attributed to some rounding of the top edges of the groove walls during the fabrication process, which significantly reduces the contribution of higher-order spatial harmonics in the magnetic potential (equation (1)). The magnitude of the B_y component is found to decrease exponentially with distance y with a decay length given approximately by $a/2\pi$ (Fig. 3(b)). In the

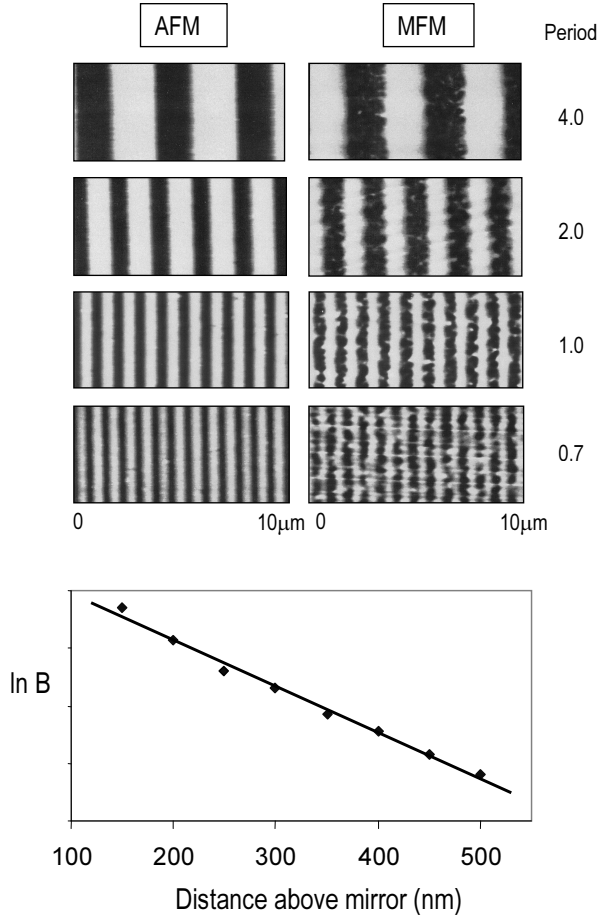


Fig. 3. (a) Atomic force microscope and magnetic force microscope scans of grooved perpendicularly magnetised $\text{Co}_{0.8}\text{Cr}_{0.2}$ microstructures with periodicities $a = 0.7, 1, 2$ and $4 \mu\text{m}$. The MFM scans were taken at a constant height of $0.05 \mu\text{m}$ above the tops of the grooves. (b) Plot of $\ln B$ versus height above the surface for the $a = 1 \mu\text{m}$ grooved magnetic microstructure. The slope yields a decay length of $0.14 \mu\text{m}$, compared with $k^{-1} = a/2\pi = 0.16 \mu\text{m}$.

regions above the protrusions, *i.e.*, at distances close ($\sim 0.05 \mu\text{m}$) to the surface, the B_y component shows evidence of domain structure, with domain sizes around $0.5 \mu\text{m}$. In the regions above the grooves, *i.e.*, at distances $y \sim 0.6 \mu\text{m}$ above the bottom surface of the grooves, the magnetic inhomogeneities associated with the domain structure are found to have decayed away, consistent with a domain size of about $0.5 \mu\text{m}$.

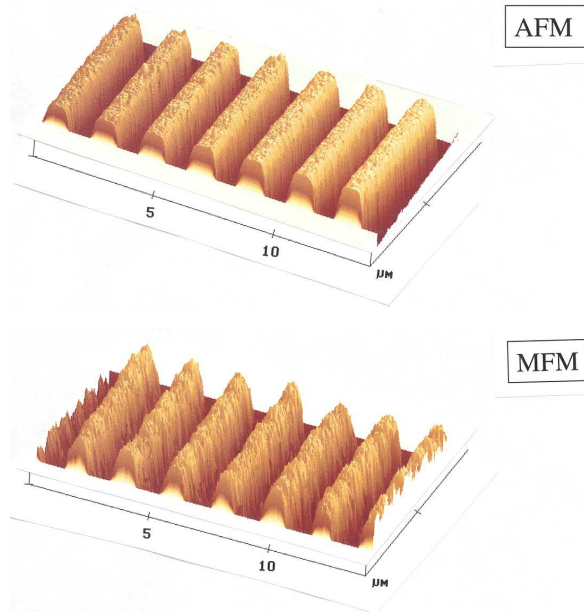


Fig. 4. Three-dimensional atomic force and magnetic force microscope scans of a grooved perpendicularly magnetised $\text{Co}_{0.8}\text{Cr}_{0.2}$ microstructure with periodicity $a = 2 \mu\text{m}$. The MFM scans were taken at a constant height of about $0.05 \mu\text{m}$ above the tops of the grooves.

Kerr-effect hysteresis curves taken for the $\text{Co}_{0.8}\text{Cr}_{0.2}$ films exhibit a rhombus rather than square shape, with a remanent magnetic field about one-quarter of the saturation field and a coercivity of about 1 kOe. The rhombus shape, which is typical of $\text{Co}_{0.8}\text{Cr}_{0.2}$ [22], implies that not all of the magnetic domains remain perfectly oriented after the magnetising process, as indicated by the MFM scans at distances close to the surface (Fig. 3(a)). The saturation magnetic field for $\text{Co}_{0.8}\text{Cr}_{0.2}$ is about 5 kG [21]; so for grooved magnetic microstructures with periodicity $a = 1 \mu\text{m}$ and $4 \mu\text{m}$ and film thickness $b = 0.2 \mu\text{m}$ the characteristic field is estimated to be $B_0 \approx 280 \text{ G}$ and 110 G, respectively. The observed approximately sinusoidal variation of B_y with x at distances close to the surface (Fig. 4) indicates that the coefficient for the third-order spatial harmonic in (1) is less than $1/3$ for these magnetic microstructures and that it should not be necessary to have characteristic fields as high as $B_0 \approx 1 \text{ kG}$ to produce a high-quality magnetic mirror with these microstructures.

The reflection of a collimated HeNe laser beam from the grooved magnetic microstructures reveals a small convex cylindrical curvature, which contributes an angular spread $\Delta\theta \approx 4 \text{ mrad}$ in the x direction and $\Delta\theta \approx 2 \text{ mrad}$

in the z direction. The small curvature is attributed to stresses in the $\text{Co}_{0.8}\text{Cr}_{0.2}/\text{Au}$ films introduced during electroplating of the thick supporting layer of copper.

2.5. Performance of the grooved magnetic microstructures

The grooved magnetic $\text{Co}_{0.8}\text{Cr}_{0.2}$ microstructures were tested by studying the reflection of a cloud of laser-cooled, σ^+ -pumped rubidium or caesium atoms dropped from a magneto-optical trap located 12–20 mm above the surface of the microstructure.

Time-of-flight absorption measurements [3] for atoms falling onto the magnetic microstructures show strong reflection signals (*e.g.*, Fig. 5 for a $a = 1 \mu\text{m}$ structure), where the reflectivity is determined essentially by the efficiency of the optical pumping of the atoms into low field-seeking mag-

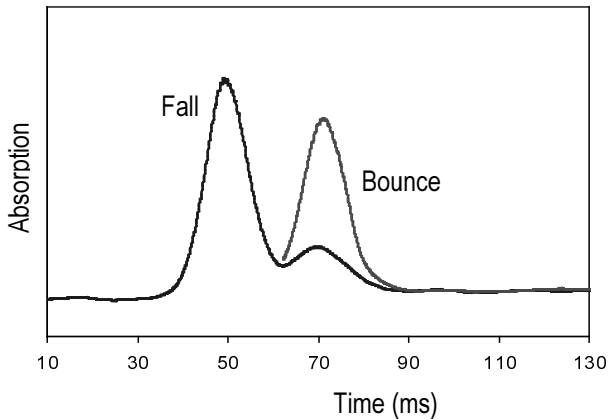


Fig. 5. Time-of-flight absorption signals for laser-cooled, σ^+ -pumped caesium atoms dropped from a height $h = 18 \text{ mm}$ onto a $a = 1 \mu\text{m}$ grooved $\text{Co}_{0.8}\text{Cr}_{0.2}$ magnetic microstructure.

netic states. Fig. 6 shows CCD images of laser-induced fluorescence signals from a cloud of rubidium atoms falling onto and bouncing from a grooved magnetic microstructure of periodicity $a = 4 \mu\text{m}$. Two bounces and three falls are clearly observed before the atoms are lost by ballistic expansion due to the transverse velocity component of the cold atoms.

Measurements of the specularity of the reflection from the $a = 1, 2$ and $4 \mu\text{m}$ grooved microstructures were made by recording the spatial distribution of the atom cloud at different times before and after reflection, with the CCD camera positioned above the atom cloud. Fig. 7 shows the width of the spatial distributions measured in the x direction

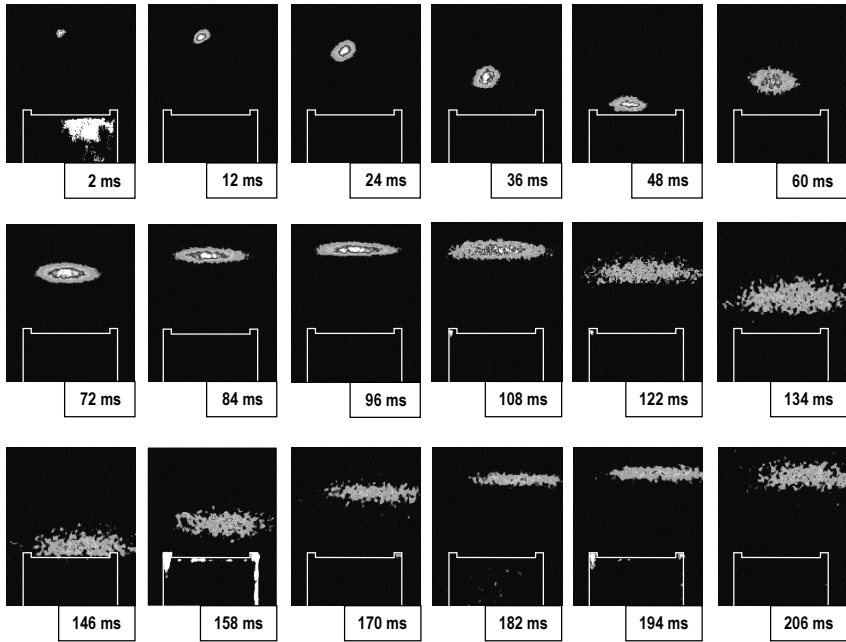


Fig. 6. Side view of laser-induced fluorescence signals from a cloud of rubidium atoms falling onto and bouncing from a grooved $\text{Co}_{0.8}\text{Cr}_{0.2}$ magnetic microstructure with periodicity $a = 4 \mu\text{m}$. Times after release from the optical molasses are shown. The drop height was 12.5 mm.

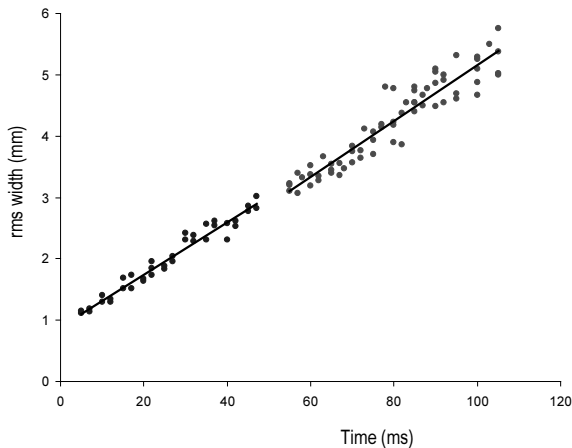


Fig. 7. Width of the expanding rubidium atom cloud as a function of time after release from the optical molasses before (left hand line) and after (right hand line) reflection from a grooved $\text{Co}_{0.8}\text{Cr}_{0.2}$ magnetic microstructure with periodicity $a = 4 \mu\text{m}$. The drop height was 12.5 mm.

(perpendicular to the grooves and the optical pumping and probe laser direction) for an $a = 4 \mu\text{m}$ microstructure as a function of time after release from the optical molasses. The slopes of straight-line fits to the width of the atom cloud give for the transverse velocity before and after reflection: $(v_{\text{rms}})_{\text{before}} = (4.27 \pm 0.30) \text{ cm s}^{-1}$ and $(v_{\text{rms}})_{\text{after}} = (4.56 \pm 0.40) \text{ cm s}^{-1}$ (where the uncertainties represent two standard errors) and a temperature of $20 \mu\text{K}$ for the atom cloud. Similar v_{rms} values were obtained from fits to the width of the atom cloud measured in the z direction (parallel to the grooves). The above results yield a value for the transverse velocity introduced by reflection of $\Delta(v_{\text{rms}}) = (1.6 \pm_{2,0}^{1,1}) \text{ cm s}^{-1}$ and an angular spread of $\Delta\theta_{\text{rms}} = (16 \pm_{20}^{11}) \text{ mrad}$. The angular spread ($\Delta\theta \approx 4 \text{ mrad}$) due to the small convex cylindrical curvature of the microstructure has an insignificant effect at the present level of uncertainty. Similar analyses, but using smaller data sets, were performed for the $a = 1$ and $2 \mu\text{m}$ magnetic microstructures.

2.6. Discussion

The above results indicate that within the present experimental uncertainties ($\approx \pm 15 \text{ mrad}$) there is no significant angular spread of the atom cloud introduced during reflection from the grooved magnetic microstructures and hence the reflection is consistent with specular reflection. To reduce the uncertainties further will require reducing the transverse velocity of the atoms by collimating the cloud of atoms or by preparing or selecting a very narrow velocity distribution by using techniques such as velocity-selective stimulated Raman transitions [23,24], or extending the spatial distribution measurements out to much longer times after the first reflection.

The quality of the grooved magnetic microstructures could be further improved by using TbGdFeCo magneto-optical films instead of CoCr. Perpendicularly magnetised TbGdFeCo films can have magnetisations as high as 3.5 kG , which for the $a = 1 \mu\text{m}$, $b = 0.2 \mu\text{m}$ magnetic microstructure would produce a characteristic surface magnetic field of about $B_0 \approx 850 \text{ G}$. Furthermore, magnetic force and atomic force microscope images taken on perpendicularly magnetised TbGdFeCo films show excellent magnetic homogeneity, with no evidence of domain structure, and a surface topological roughness of less than 1 nm .

When the microstructure is used as a diffractive beam splitter the angular spread $\Delta\theta_{\text{rms}}$ introduced by the reflection needs to be smaller than the splitting of the first-order diffraction peak $\theta_{\text{diff}} = \lambda_{\text{dB}}/(a \sin \alpha)$, where $\lambda_{\text{dB}} = h/Mv$ is the atomic de Broglie wavelength, Mv is the atomic momentum, and α the angle of incidence (defined from the horizontal). For $\alpha = 20^\circ$ (which is close to the optimum for diffraction from a magnetic grating [4]), $v = 0.5 \text{ cm s}^{-1}$ (corresponding to a drop height $h = 13 \text{ mm}$), $M = 87 \text{ amu}$ and $a = 1 \mu\text{m}$, the de Broglie wavelength is 10 nm and the

diffraction angle $\theta_{\text{diff}} = 28$ mrad. Thus, in order to resolve the zero and first orders, the angular spread $\Delta\theta_{\text{rms}}$ needs to be less than about 15 mrad. When the microstructure is used as an optical element in an atom interferometer the transverse coherence length of the atom after reflection should be longer than the path length in the interferometer, in order for the interference fringes to have good visibility. Thus, for a path length of 20 mm and $\lambda_{\text{dB}} = 10$ nm, the angular spread $\Delta\theta_{\text{rms}}$ needs to be less than about 1 mrad.

3. Integrated magnetic atom optics

We are exploring the use of permanent magnet microstructures based on the magnetic microstructure technology developed for the grooved magnetic mirrors to construct miniature integrated atom optical elements, including magnetic waveguides, microtraps and beam splitters, for manipulating atomic de Broglie waves on the surface of a substrate [17].

3.1. Miniature surface waveguides and beam splitters

We first consider the magnetic field distribution produced by a *single* perpendicularly magnetised thin magnetic strip, of width $2w$, thickness b located in the x - z plane with infinite extension along z , on the surface of a substrate. The components of the magnetic field (in SI units) are given by [17]

$$B_x(x, y) = \frac{B_0}{8} \ln \frac{[y^2 + (x - w)^2] [(y - b)^2 + (x + w)^2]}{[y^2 + (x + w)^2] [(y - b)^2 + (x - w)^2]}, \quad (4a)$$

$$B_y(x, y) = \frac{B_0}{4} \tan^{-1} \frac{2bw [y(y - b) - x^2 + w^2]}{[x^2 + y(y - b) + w^2]^2 + b^2(x^2 - w^2) - 4x^2w^2}, \quad (4b)$$

where $B_0 = 2\mu_0 M_0/\pi$, and M_0 is the magnetisation. The single magnetic strip, when combined with a bias magnetic field B_{bias} (*e.g.*, from a pair of Helmholtz coils), can produce a 2D quadrupole potential above the substrate (Figs. 8(a) and 8(b)). Atoms in low field-seeking magnetic states are attracted towards the minimum of the magnetic potential, allowing 2D trapping and the formation of a guiding tube for cold atoms. If the characteristic size of the 2D quadrupole trap is comparable with the de Broglie wavelength of the atoms then such a device can act as a surface waveguide for atoms.

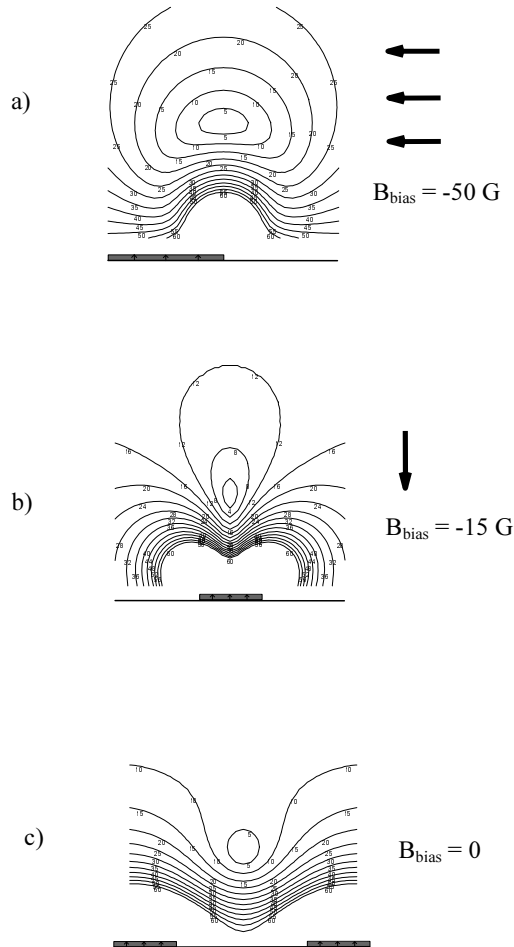


Fig. 8. Calculated magnetic field distributions for three types of perpendicularly magnetised thin-film waveguides. (a) Single-magnet strip of semi-infinite width with horizontal bias field. (b) Single-magnet strip of width $20 \mu\text{m}$ with vertical bias field. (c) Two magnetic strips of width $20 \mu\text{m}$ and separation $80 \mu\text{m}$ (between centres) with no bias field. The magnetic films are $1 \mu\text{m}$ thick and the magnetisation $M_0 = 1.25 \text{ kG}$.

Fig. 8(a) shows the calculated magnetic field distribution for a single perpendicularly magnetised strip with semi-infinite width, $b = 1 \mu\text{m}$, $M_0 = 1.25 \text{ kG}$ (typical for $\text{Co}_{0.8}\text{Cr}_{0.2}$) and a horizontal bias field $B_{\text{bias}} = -50 \text{ G}$. These parameters produce a 2D quadrupole trap located $50 \mu\text{m}$ above the edge of the magnetic strip with a magnetic field gradient of 10 kG cm^{-1} . Fig 8(b) shows the magnetic field distribution for a single magnetic strip

waveguide, with $2w = 20 \mu\text{m}$, $b = 1 \mu\text{m}$ and a vertical bias field $B_{\text{bias}} = -15 \text{ G}$. This configuration produces a 2D quadrupole trap located $40 \mu\text{m}$ above the centre of the magnetic strip with a magnetic field gradient of 20 kG cm^{-1} . Raising the bias field to $B_{\text{bias}} = -50 \text{ G}$ lowers the centre of the trap to $7.5 \mu\text{m}$ above the substrate and increases the magnetic field gradient to 90 kG cm^{-1} .

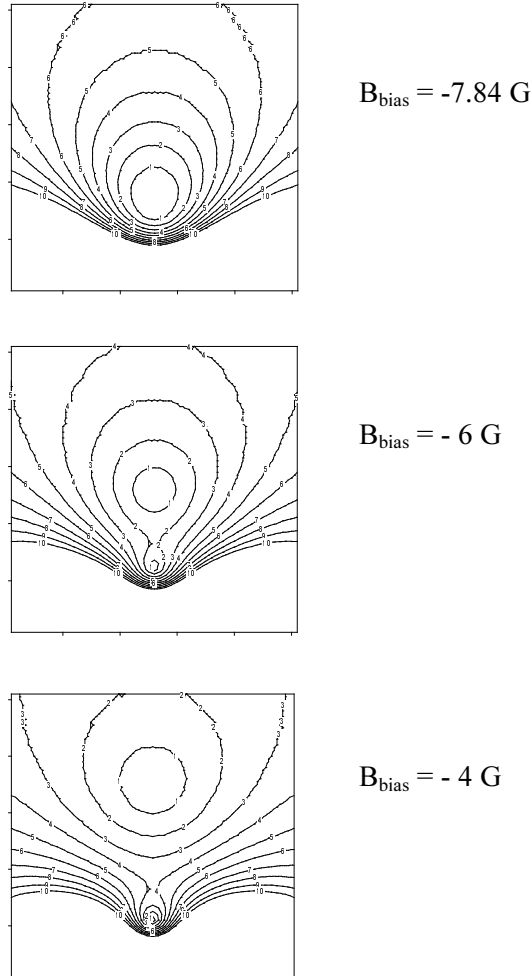


Fig. 9. Effect of a bias magnetic field on the double-magnet waveguide (Fig. 8(c)) in the vicinity of a macroscopic quadrupole trap with magnetic field gradient 50 G cm^{-1} . The two traps merge for a bias field of -7.84 G , demonstrating the principle of a beam recombiner or beam splitter. The magnetic films in the double-magnet waveguide are $20 \mu\text{m}$ wide, $1 \mu\text{m}$ thick, and separated by $80 \mu\text{m}$ (between centres). The magnetisation is 1.25 kG .

A magnetic microstructure comprising two separated magnetic strips produces a 2D quadrupole potential without the need for a bias field. Fig. 8(c) shows the magnetic field distribution for two perpendicularly magnetised strips with mid-points separated by $80\ \mu\text{m}$, $2w = 20\ \mu\text{m}$, $b = 1\ \mu\text{m}$ and $M_0 = 1.25\ \text{kG}$. When a vertical bias magnetic field is applied to the magnetic microstructure the 2D quadrupole trap can be moved up and down and made to merge with or separate from a second quadrupole trap. Such a device can act as a beamsplitter or recombiner for cold atoms, as illustrated in Fig. 9.

3.2. Surface magnetic microtraps

A combination of a two-strip magnetic waveguide, a bias magnetic field and a pair of wires carrying current in the same direction to generate a small guiding magnetic field can produce a novel type of 2D Ioffe–Pritchard (IP) microtrap for coupling cold atoms from a conventional Magneto–Optical Trap (MOT) or a mirror MOT [18] into a surface magnetic waveguide

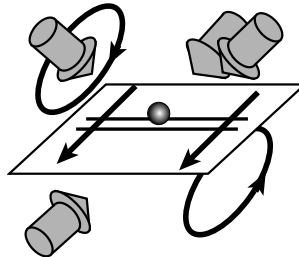


Fig. 10. Mirror magneto–optical trap and a two-dimensional Ioffe–Pritchard microtrap comprising two magnetic strips (parallel lines), a bias magnetic field and a pair of wires (parallel arrows) carrying current in the same direction.

(Fig. 10). The microtrap has a small capturing volume; so the atoms are first loaded from a MOT or mirror MOT into the quadrupole magnetic trap produced by the MOT coils and then adiabatically transferred to a macroscopic IP magnetic trap formed by a Z-shaped millimetre-sized wire mounted beneath the substrate (Fig. 10) [18]. The cold atoms can then be loaded into the 2D IP microtrap by varying the bias magnetic field to allow the minimum of the macroscopic trap to merge with the minimum of the surface IP microtrap (Fig. 11). By altering the bias field and implementing evaporative cooling the atoms may be transferred to within about $10\ \mu\text{m}$ of the substrate with a view to achieving a Bose condensate.

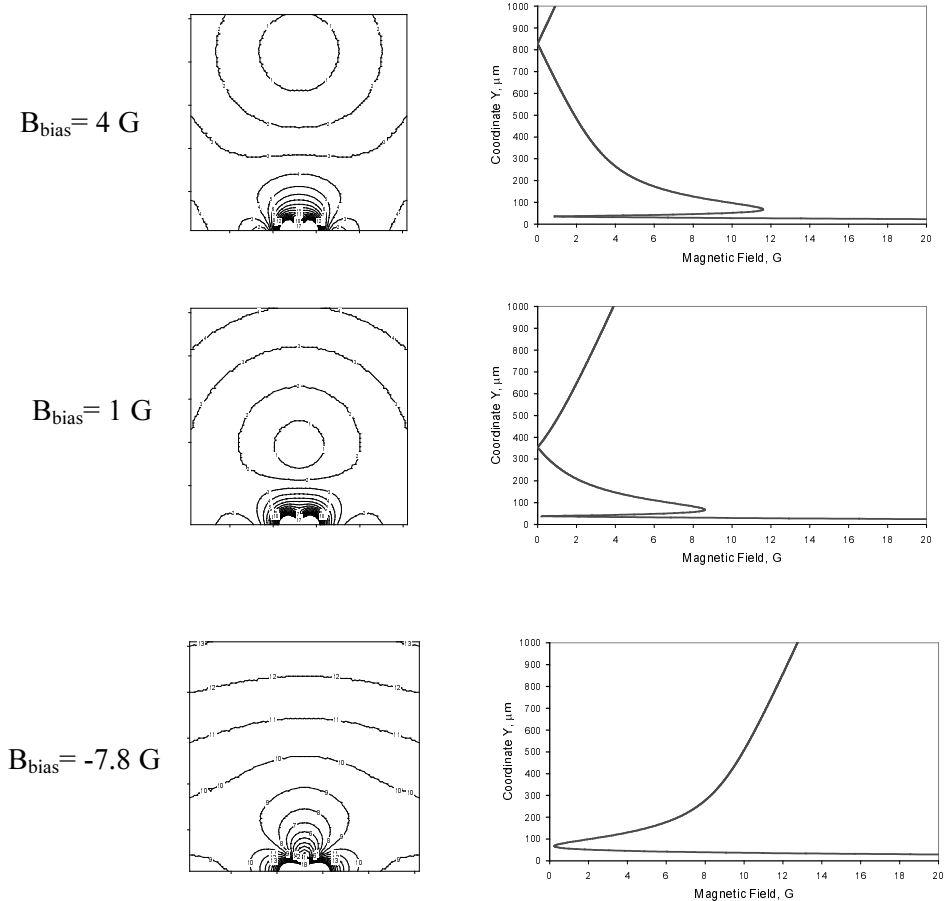


Fig. 11. Scheme for loading cold atoms from a macroscopic quadrupole trap (magnetic field gradient 50 G cm^{-1}) into a double-magnet waveguide (Fig. 8(c)) by adjusting the bias magnetic field. The magnetic films in the waveguide are $20 \mu\text{m}$ -wide, $1 \mu\text{m}$ -thick, and separated by $80 \mu\text{m}$ (between centres). The magnetisation is 1.25 kG .

3.3. Discussion

It has recently been demonstrated that miniature surface-mounted optical elements based on lithographically-patterned current-carrying microcircuits [18, 25–28] have certain advantages over macroscopic free-standing optical elements for manipulating cold atoms. The use of current-carrying microcircuits allows the fabrication of networks of microtraps, waveguides and couplers. Scaling down the dimensions of the optical elements and using surface-mounted microdevices allow the use of moderate electric currents

and provides improved optical access. The magnetic field gradient and curvature scale as M/l^2 and M/l^3 , respectively (where l is the characteristic size of the structure); so surface-mounted microdevices can provide large magnetic field gradients and very tight confinement of the atomic de Broglie waves. The tight confinement increases the elastic collision rate and can speed up Bose–Einstein condensation, allowing condensates to be produced more easily and in more modest vacuums [29,30]. The vibrational quantum level splitting in the microtraps can be larger than the photon-recoil energy (Lamb–Dicke regime), allowing occupation of a single vibrational quantum state.

Magnetic microstructures fabricated from permanent magnetic films have potential advantages over current-carrying microcircuits. Permanent magnetic films can have large magnetisation ($M_0 \sim 10$ kG) and can be fabricated into very fine microstructures ($\sim 1 \mu\text{m}$), allowing, in principle, magnetic field gradients as large as 10^8 G cm $^{-1}$. Permanent magnetic microstructures can also be fabricated with much larger overall dimensions than microcircuits. Finally, permanent magnetic film devices avoid problems associated with excessive heating at high current densities, noise due to current variations, imperfect insulation and current leakages, and open and short circuits.

For atoms in tightly confined microtraps and waveguides, consideration needs to be given to surface–atom interactions. Surface-induced heating has been studied theoretically [31] and is predicted to become important at distances around $10 \mu\text{m}$. Decoherence due to coupling of the atoms to the environment and dephasing due to magnetic fields are also important issues that need to be investigated.

4. Summary and future perspectives

A new type of magnetic mirror based on *grooved*, perpendicularly magnetised microstructures fabricated by electron-beam lithography has been constructed, characterised and tested. Strong reflection signals and predominantly specular reflection have been realised for beams of cold caesium or rubidium atoms normally incident on grooved magnetic microstructures with periodicity ranging from $1\text{--}4 \mu\text{m}$. The accuracy of the specular measurements ($\delta(\Delta\theta_{\text{rms}}) \approx \pm 15$ mrad), which is currently limited by the transverse velocity of the atoms, could be improved significantly by collimating the cloud of atoms or by preparing or selecting a narrow velocity distribution. This type of grooved magnetic microstructure appears to be the most promising approach to date for producing high-quality magnetic optical elements with micron-scale periodicity.

The magnetic microstructure technology is currently being extended to the development of miniature integrated atom optical elements, including magnetic waveguides, microtraps and beamsplitters, which will be used to construct an integrated atom interferometer on the surface of a substrate. Such a surface-based atom interferometer should be more suitable than free-standing atom interferometers for operation on a moving platform as a sensor of gravity fields and gravity gradients.

We thank P.L. Larkins, R.A. Lee, X. Yang, J.P. Hayes and E.C. Harvey for their contributions to the fabrication of the grooved magnetic microstructures, J. Koperski for his contributions during the early stages of this project and the CSIRO Manufacturing Science and Technology for use of the laser cooling equipment. The integrated atom optics project is supported by an Australian Research Council Discovery Grant. We dedicate this paper to the memory of our friend and colleague Professor Geoffrey Opat.

REFERENCES

- [1] G.I. Opat, S.J. Wark, A. Cimmino, *Appl. Phys.* **B54**, 396 (1992).
- [2] T.M. Roach, H. Abele, M.G. Boshier, H.L. Grossman, K.P. Zetie, E.A. Hinds, *Phys. Rev. Lett.* **75**, 629 (1995).
- [3] A.I. Sidorov, R.J. McLean, W.J. Rowlands, D.C. Lau, J.E. Murphy, M. Walkiewicz, G.I. Opat, P. Hannaford, *Quant. Semiclass. Opt.* **8**, 713 (1996).
- [4] T.J. Davis, *Eur. J. Phys.* **D14**, 111 (2001).
- [5] G.I. Opat, S. Nic Chormaic, B.P. Cantwell, J.A. Richmond, *J. Opt. B: Quant. Semiclass. Opt.* **1**, 415 (1999).
- [6] C.J. Myatt, N.R. Newbury, R.W. Guist, S. Luitzenhiser, C.E. Wieman, *Opt. Lett.* **21**, 290 (1996).
- [7] J.A. Richmond, S. Nic Chormaic, B.P. Cantwell, G.I. Opat, *Acta Phys. Slovaca* **48**, 481 (1998).
- [8] J.A. Richmond, B.P. Cantwell, S. Nic Chormaic, D.C. Lau, A.M. Akulshin, G.I. Opat, *Phys. Rev.* **A65**, 033422 (2002).
- [9] I.G. Hughes, P.A. Barton, T.M. Roach, M.G. Boshier, E.A. Hinds, *J. Phys. B* **30**, 647 (1997).
- [10] C.V. Saba, P.A. Barton, M.G. Boshier, I.G. Hughes, P. Rosenbusch, E.A. Hinds, *Phys. Rev. Lett.* **82**, 468 (1999).
- [11] D.S. Gough, R.J. McLean, A.I. Sidorov, D.C. Lau, J. Koperski, W.J. Rowlands, B.A. Sexton, G.I. Opat, P. Hannaford, *Laser Spectroscopy*, Eds. R. Blatt, J. Eschner, D. Leibfried, F. Schmidt-Kaler, World Scientific, Singapore 1999, p. 340.

- [12] D.C. Lau, R.J. McLean, A.I. Sidorov, D.S. Gough, J. Koperski, W.J. Rowlands, B.A. Sexton, G.I. Opat, P. Hannaford, *J. Opt. B: Quant. Semiclass. Opt.* **1**, 371 (1999).
- [13] D.C. Lau, A.I. Sidorov, G.I. Opat, R.J. McLean, W.J. Rowlands, P. Hannaford, *Eur. J. Phys.* **D5**, 193 (1999).
- [14] M. Drndić, G. Zabow, C.S. Lee, J.H. Thywissen, K.S. Johnson, M. Prentiss, R.M. Westervelt, P.D. Featonby, V. Savalli, L. Cognet, K. Helmersen, N. Westbrook, C.I. Westbrook, W.D. Phillips, A. Aspect, *Phys. Rev.* **60**, 4012 (1999).
- [15] A.I. Sidorov, R.J. McLean, B.A. Sexton, D.S. Gough, T.J. Davis, A.M. Akulshin, G.I. Opat, P. Hannaford, *Comptes Rendus 2*, Series IV, 565 (2001).
- [16] A.I. Sidorov, D.C. Lau, G.I. Opat, R.J. McLean, W.J. Rowlands, P. Hannaford, *Laser Spectroscopy*, Eds. Z.-J. Wang, Z.-M. Zhang, Y.-Z. Wang, World Scientific, 1998, p. 252.
- [17] T.J. Davis, *J. Opt. B: Quant. Semiclass. Opt.* **1**, 408 (1999).
- [18] J. Reichel, W. Hänsel, T.W. Hänsch, *Phys. Rev. Lett.* **83**, 3398 (1999).
- [19] W.J. Rowlands, D.C. Lau, G.I. Opat, A.I. Sidorov, R.J. McLean, P. Hannaford, *Opt. Commun.* **126**, 55 (1966).
- [20] L.D. Landau, E.M. Lifshitz, *Electrodynamics of Continuous Media*, Oxford, Clarendon, 1960, p. 161.
- [21] A.I. Sidorov, D.C. Lau, G.I. Opat, R.J. McLean, W.J. Rowlands, P. Hannaford, *Laser Physics*, **8**, 642 (1998).
- [22] See, e.g., D.S. Bloomberg, G.A.N. Connell, M. Mansuripur, *Magnetic Recording Technology*, Eds. C.D. Mee and E.D. Daniels, McGraw-Hill, New York 1988.
- [23] M. Kasevich, D. Weiss, E. Riis, K. Moler, S. Kasapi, S. Chu, *Phys. Rev. Lett.* **66**, 2297 (1991).
- [24] V. Savalli, D. Stevens, J. Estève, P.D. Featonby, V. Josse, N. Westbrook, C.I. Westbrook, A. Aspect, [arXiv:physics/0202059](https://arxiv.org/abs/physics/0202059).
- [25] D. Müller, D.Z. Anderson, R.J. Grow, P.D.D. Schwindt, E.A. Cornell, *Phys. Rev. Lett.* **83**, 5194 (1999).
- [26] R. Folman, P. Krüger, D. Cassettari, B. Hessmo, T. Maier, J. Schmiedmayer, *Phys. Rev. Lett.* **84**, 4749 (2000).
- [27] N.H. Decker, C.S. Lee, V. Lorent, J.H. Thywissen, S.P. Smith, M. Drndić, R.M. Westervelt, M. Prentiss, *Phys. Rev. Lett.* **84**, 1124 (2000).
- [28] E.A. Hinds, C.J. Vale, M.G. Boshier, *Phys. Rev. Lett.* **86**, 1462 (2001).
- [29] W. Hänsel, P. Hommelhoff, T.W. Hänsch, J. Reichel, *Nature* **413**, 498 (2001).
- [30] H. Ott, J. Fortagh, G. Schlotterbeck, A. Grossmann, C. Zimmermann, *Phys. Rev. Lett.* **87**, 230401 (2001).
- [31] C. Henkel, S. Pötting, M. Wilkins, *Appl. Phys.* **B69**, 379 (1999).